Scanning Microscopy

Volume 10 | Number 3 Article 6

4-11-1996

Tc-Mapping and Investigation of Water-Initiated Modification of YBa2Cu3O7-x Thin Films by Low Temperature Scanning Electron Microscopy

A. V. Bobyl
State Technical University

M. E. Gaevski
Physico-Technical Institute, megay@charm.pti.spb.su

S. G. Konnikov
Physico-Technical Institute

D. V. Shantsev
State Technical University

V. A. Solov'ev
Physico-Technical Institute

Tc-Mapping and Investigation of Water-Initiated Modification of YBa2Cu3O7-x Thin Films by Low Temperature Scanning Electron Microscopy

Authors

A. V. Bobyl, M. E. Gaevski, S. G. Konnikov, D. V. Shantsev, V. A. Solov'ev, and R. A. Suris

Scanning Microscopy, Vol. 10, No. 3, 1996 (Pages 679-695) 0891-7035/96$5.00+.25
Scanning Microscopy International, Chicago (AMF O'Hare), IL 60666 USA

T_c-MAPPING AND INVESTIGATION OF WATER-INITIATED MODIFICATION OF $YBa_2Cu_3O_{7-x}$ THIN FILMS BY LOW TEMPERATURE SCANNING ELECTRON MICROSCOPY

A.V. Bobyl, M.E. Gaevski[1*], S.G. Konnikov[1], D.V. Shantsev, V.A. Solov'ev[1] and R.A. Suris[1]

Chair of Solid State Physics, State Technical University, 29 Polytechnicheskaya, St. Petersburg 195251, Russia
[1]A.F.Ioffe Physico-Technical Institute, 26 Polytechnicheskaya, St. Petersburg 194021, Russia

(Received for publication May 8, 1995 and in revised form April 11, 1996)

Abstract

The T_c-mapping method using low temperature scanning electron microscopy (LTSEM) has been developed to study the spatial distribution of the critical temperature in high temperature superconducting (HTSC) films with a spatial resolution approaching 2 μm. To achieve so high a spatial resolution, a numerical deconvolution method was applied that eliminated distorting effects associated with the thermal diffusion and with the contribution from the absorbed beam current. The T_c-mapping method was used to investigate modification by water of $YBa_2Cu_3O_{7-x}$ films grown on (100) MgO and (110) $LaAlO_3$ substrates. The rate of modification of a [110]-oriented $YBa_2Cu_3O_{7-x}/LaAlO_3$ film is found to be 40 times that of a c-axis oriented $YBa_2Cu_3O_{7-x}$/MgO epitaxial film. It is argued that water-initiated modification of the films results from penetration of hydrogen into the films, rather than from out-diffusion of oxygen.

Key Words: Low-temperature scanning electron microscopy, electron beam induced voltage, high-T_c superconductors, water-initiated modification, thin films, T_c-distribution function, $YBa_2Cu_3O_{7-x}$, current distribution inhomogeneities, morphology, mapping.

*Address for correspondence:
M.E. Gaevski
A.F. Ioffe Physico-Technical Institute,
Polytechnicheskaya 26,
St. Petersburg 194021,
Russia

Telephone number: (812) 247 93 82
FAX number: (812) 247 10 17
E.mail: megay@charm.pti.spb.su

Introduction

In contrast to conventional superconductors which have a very narrow superconducting transition region ($\sim$ 0.1K), the transition region in high temperature superconducting (HTSC) materials is substantially broadened because of their strong inhomogeneity. The inhomogeneity of thin HTSC films is caused both by the complicated structure of the materials themselves and by the influence of substrate, involving lattice mismatch, difference in thermal expansion coefficients, and chemical interaction. The inhomogeneity is especially strong in the case of films grown on MgO or $LaAlO_3$ substrates which are widely used in microwave devices.

Some information about the quality of a thin HTSC film can be extracted from the temperature dependence of its resistance and from its current-voltage characteristic. However, ordinary measurement methods give values of the superconducting parameters (critical temperature T_c, width of the superconducting transition region ΔT_c, critical current density j_c) averaged over the entire film area. This information is insufficient to recognize the nature of defects responsible for the non-uniformity of transport properties and for the broadening of the superconducting transition region. Identification and investigation of these defects can be very helpful in getting better insight into various aspects of high-T_c superconductivity and in improving the film quality and characteristics of HTSC devices. Thus, it is very important to perform local investigations of HTSC films, which could provide information on local superconducting properties.

One of the most powerful tools for a local study of HTSC thin films and thin film devices is the low temperature scanning electron microscopy (LTSEM). This method was first developed by Prof. Huebener and his co-workers to study conventional superconductors (Clem and Huebener, 1980; Huebener, 1987) and was applied to HTSC films (Huebener *et al.*, 1988). LTSEM technique has since been used for visualization of regions with different T_c (Koelle *et al.*, 1990; Umansky *et al.*, 1990) or those with different j_c (Gross *et al.*, 1989b), as well as for studying Josephson junctions formed on grain

boundaries in bicrystalline and polycrystalline films (Mannhart *et al.*, 1989). To perform a quantitative analysis of various phenomena in HTSC films (current percolation, degradation of superconducting properties, etc.), it is necessary to obtain, with high spatial resolution, quantitative information about the spatial distribution of T_c and ΔT_c.

Several papers have reported on measurements of local superconducting parameters T_c, ΔT_c and j_c in thin HTSC films by LTSEM (for a review, see Gross and Koelle, 1994). In these papers the spatial resolution was supposed to be 1-2 μm. As will be shown below (under **Distorting effects**), this may be true only in the case of j_c measurements carried out at temperature $T < T_c$, while in investigations of the spatial distribution of critical temperature, only a very low spatial resolution can be achieved which is determined by peculiarities of thermal diffusion.

Our investigations employing the LTSEM technique reported in this paper represent the first step in determining the map of critical temperatures for an HTSC film. To improve the spatial resolution of LTSEM, a numerical deconvolution method has been developed which eliminates the distorting effects associated with the thermal diffusion and contribution from the absorbed beam current. The best results obtained by now are two-dimensional T_c-maps with a T_c-resolution of about 0.2K and spatial resolution of about 2 μm. The T_c-maps were measured for areas of up to 25000 μm^2.

The effects of ambient atmospheric conditions and various other environmental factors on HTSC materials have been widely investigated (Barns and Laudise, 1987; Nishihara *et al.*, 1988; Jandl *et al.*, 1989). When looking for an object to be studied by the technique of T_c-mapping, we found that modification of HTSC films by water is quite promising as a process to be controlled. In this work, water-initiated modification of $YBa_2Cu_3O_{7-x}$ (YBaCuO) films grown on (100) MgO and (110) $LaAlO_3$ substrates has been investigated. It is shown that storage in water may increase the T_c of YBaCuO films by as much as 2K. The evolution of a local-T_c ensemble is calculated for different films. The data obtained suggest hydrogenation of YBaCuO film as a mechanism of water-initiated modification. The results of hydrogenation are discussed in terms of an effective change of oxygen deficiency.

The fundamentals of LTSEM

One more advantage of LTSEM, in addition to its high spatial resolution, is the possibility to simultaneously record and compare directly different signals. For example, different kinds of information on superconducting properties of HTSC films (electron beam induced voltage: EBIV mode), their morphology (secondary electrons: SE mode) and chemical composition (backscattered electrons: BSE mode) can be obtained.

In the present work, we have improved the LTSEM technique, specifically, the method using EBIV, so as to carry out quantitative studies of the T_c-spatial distribution in HTSC films with really high spatial resolution.

The principal idea of the EBIV method (Clem and Huebener, 1980) is as follows. The film surface is scanned by the electron beam of a scanning electron microscope (SEM), while the bottom side of the substrate is in direct contact with a sample mounting stage, which allows operating temperatures to be maintained in the interval from 77K up to 273K. A standard four-contact scheme is used. Heating a local region by the electron beam irradiation elevates its temperature by ΔT, which causes a change $\Delta\rho(T,r)$ in the local resistivity ρ. As a result, there occurs a change S(T) in the voltage across the microbridge, while the total current I_{tot} passed through the sample is held constant. The EBIV signal thus obtained is given by:

$$S(T) = \{\delta P/I_{tot}\} = \{[\delta \int \rho(r) j^2(r) dV]/I_{tot}\} = \{[\int j^2(r) \Delta\rho(r) dV]/I_{tot}\} \quad (1)$$

where δP is the electron beam induced change of electric power, j is the current density. It is readily shown that eq. (1) is valid for $\Delta\rho(T) << \rho(T)$ (Butterweck, 1975). In the case of only a slight increase in local temperature due to irradiation ($\Delta T << \Delta T_c$) one obtains $\Delta\rho(T) = (\partial\rho/\partial T)\Delta T$. Thus, eq. (1) can be simplified:

$$S(T,x,y) \propto j^2(T,x,y) \{\partial\rho(T,x,y)/\partial T\}. \quad (2)$$

The method gives EBIV as a function of either temperature or the coordinate point (x,y) of the electron beam focus on the film surface.

The temperature dependence of the EBIV signal S(T) gives information on the local characteristics of the superconducting transition (Huebener *et al.*, 1988). This is shown schematically in Figure 1 with local transition curves $\rho(T)$ and corresponding S(T) dependencies for three film fragments with different values of T_c. It follows from eq. (2) that in the simplest case, when $j \sim$ constant, the local EBIV signal S(T) is a direct measure of the temperature derivative of the local resistivity $\rho(T)$ (Koelle *et al.*, 1990). Actually, the S(T) peak position strongly depends on the T_c value of the irradiated region, and the width of the S(T) peak is related to the width of the local transition region. If $\Delta T \approx \Delta T_c$, the local curves $\rho(T)$ can be obtained by a reconstruction procedure detailed by Konnikov *et al.* (1992).

In the low temperature part of the superconducting transition region ($\rho \to 0$), the change in local resistivity may exceed the value of ρ. Besides, the voltage-current

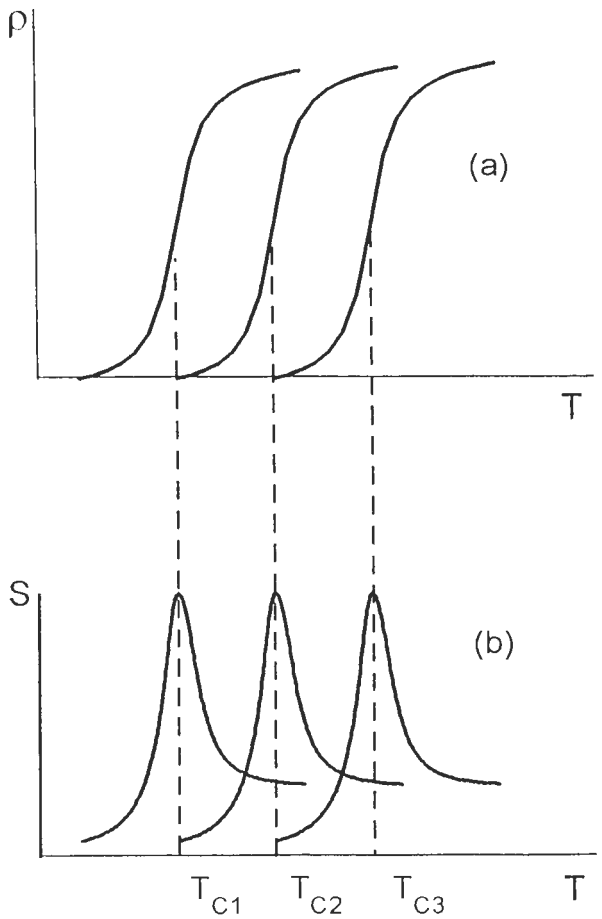

Figure 1. Sketch of the local resistivity ρ (**a**) and the EBIV signal S (**b**) versus temperature (T) for three regions with different critical temperature T_c (from Huebener *et al.*, 1988).

---

characteristics of HTSC films become strongly non-linear at these temperatures. Under these conditions, the current is completely forced out of the beam-irradiated region to the neighboring regions. Then, EBIV signal S(T) can be described in the same way as it was done by Gross and Koelle (1994):

$$S(T) = (\partial U/\partial I)\, \delta I, \qquad (3)$$

where $(\partial U/\partial I)$ is the differential resistance of a sample cross-section that includes the irradiated region and δI is the electron beam-induced change in the current flowing through the irradiated region.

In this case, the EBIV image obtained in the (x,y)-plane allows visualization of the spatial distribution of the current density over the film at a given temperature. In addition, the type of film defects such as grain boundaries, cracks, scratches and inclusions with different orientation or composition can be identified using SE and BSE modes. An EBIV image of the current distribution around these defects can clarify their nature and reveal the manner in which they control the transport properties of the film. In addition, if the pattern of current distribution inhomogeneities is known, various parameters of the film, such as, critical current density (Gross *et al.*, 1989b) and Hooge-parameter (Bobyl *et al.*, 1995) can be estimated more realistically.

Distorting Effects

Influence of temperature "tails"

LTSEM has been shown to have a high spatial resolution of about 1-2 μm (Huebener *et al.*, 1988; Gross *et al.*, 1989a; Koelle *et al.*, 1990). During the elaboration of our T_c-mapping technique, we have found that the spatial resolution may be significantly poorer. For example, when a meander-shaped series of microbridges prepared on the MgO substrate was viewed in EBIV mode, the images of neighboring microbridges were not resolved, although the distance between them was 50 μm (see Figs. 2a and 2b). The profile of the EBIV signal along a linear scan of the beam across a narrow microbridge isolated from other microbridges is plotted in Figure 3. Apart from the regions of a sharply decreasing signal intensity near the microbridge edges, the profile shows long "tails". The interference of these tails in the case of a meander structure leads to a substantial EBIV signal (comparable to that observed in the microbridge area) in the regions between the microbridges, i.e., at the points where there is no superconducting material.

We emphasize that the spatial resolution limit (SRL) may be different depending on, e.g., whether the image of an inhomogeneous film is studied in EBIV mode or an accurate measurement of local superconducting parameters is performed. Furthermore, the SRL for the case when j_c-distribution is determined, will be different from the spatial resolution limit for the case of T_c-distribution measurements.

Obviously, the spatial resolution in EBIV mode is determined by the spatial distribution of the electron-beam-induced temperature rise $\Delta T(r)$. It has been shown (Gross *et al.*, 1989a) that, on one hand, the temperature profile $\Delta T(r)$ depends on the electron range R_e and, on the other, it is determined by thermal diffusion processes. The R_e specifies the region of primary electron energy dissipation. Gross *et al.* (1989a) have also demonstrated that the SRL is mainly determined by R_e and, at $r > R_e$, the temperature rise is inversely proportional to distance.

The existence of long "tails" in $\Delta T(r)$ leads to a temperature dependence of SRL in EBIV mode. Indeed, a large area where the electron beam induced resistivity $\Delta\rho$ is not too low, makes a significant contribution to the EBIV signal attributed to the local region. The size of

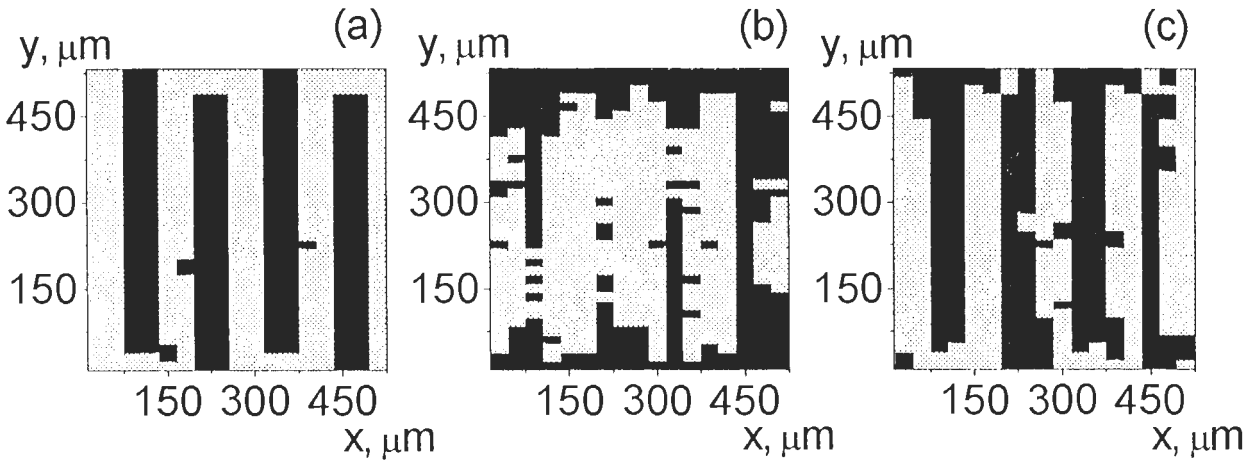

Figure 2. Digital images of a meander-shaped series of YBaCuO/MgO microbridges in (**a**) BSE mode and in (**b** and **c**) EBIV mode before (**b**) and after (**c**) the treatment that eliminates the influence of the temperature "tails" on the EBIV signal. The black level is 50%.

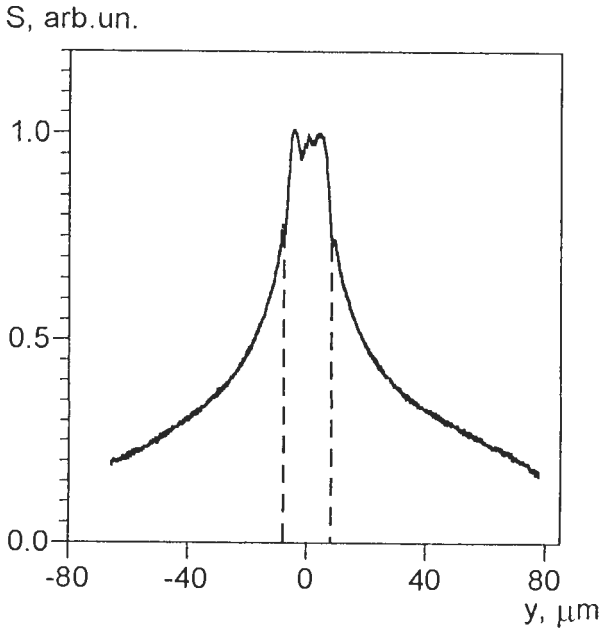

Figure 3. EBIV signal along a linear scan of the electron beam across a YBaCuO/MgO microbridge at T = T_c (T_c = 89.3K, ΔT_c = 1.1K). Dashed lines point the coordinates of the microbridges edges.

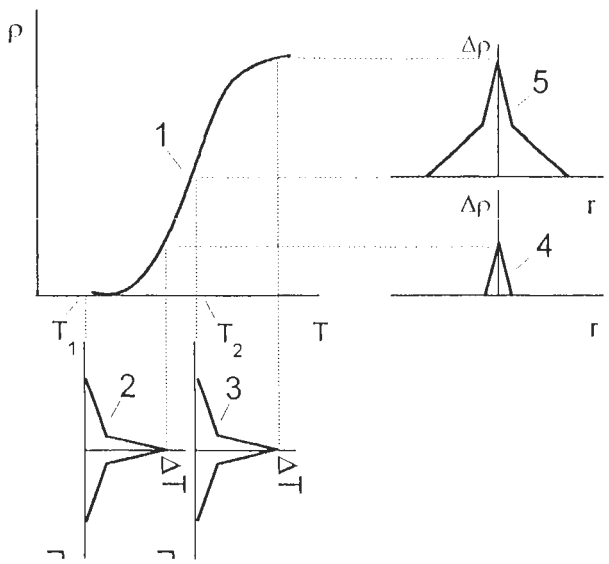

Figure 4. Sketch illustrating the temperature dependence of SRL: the temperature dependence of resistivity ρ(T) (**1**), the coordinate profiles of the electron beam induced temperature rise ΔT(r) for two temperatures T_1 (**2**) and T_2 (**3**) and the corresponding coordinate profiles of the electron beam induced resistivity $\Delta\rho(r)$ (**4**, **5**).

---

this area depends not only on the electron beam parameters and the thermal conductivity of substrate, but also on the shape of the local transition curve ρ(T) and the actual temperature.

To clarify the temperature dependence of SRL, we use a schematic sketch shown in Figure 4. Let us consider the simplest case of a homogeneous film, i.e., ρ(r) = constant. If the actual temperature T = T_1 is below T_c^{off}, the size of the region with $\Delta\rho > 0$ is mainly determined by the range R_e, being equal to about 1 μm (Fig. 4, curve 4). At the same time, for T = T_2 ($T_c^{off} < T_2 < T_c^{on}$), the size of the region with $\Delta\rho > 0$ is determined by the ΔT(*r*) - "tails" (Fig. 4, curve 5). Thus, if a j_c-spatial distribution is studied at T $\leq T_c^{off}$, the spatial resolution is as high as $\sim$1 μm, whereas in the case of a T_c-spatial distribution, when measurements throughout the superconducting transition are necessary, it is significantly worse. In order to improve the resolution, in the latter case up to few μm, a special treatment of the EBIV data should be carried out.

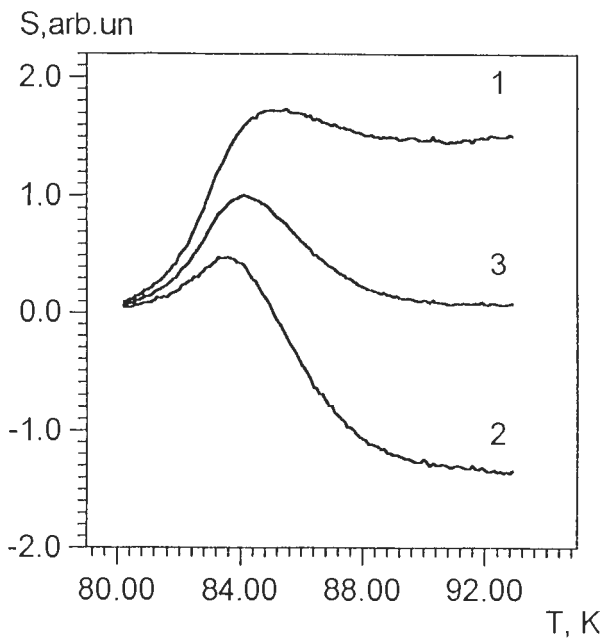

Figure 5. Temperature dependencies of the EBIV signal $S_+(T)$ (**1**), $S_-(T)$ (**2**) and S(T) (**3**) obtained on a bolometer YBaCuO/MgO structure.

The procedure used in this paper for the EBIV data treatment is as follows. Taking into account the spreading of the electron beam induced perturbation, one can write the EBIV signal measured at some coordinate point (x,y) as

$$S(x,y) = \int \Delta T(x-x',y-y')\, S_0(x',y')dx'dy' \qquad (4)$$

where

$$S_0(x',y') = \lim \{S(x',y') / (\Delta T(x',y')\Delta x'\Delta y')\}$$

at ΔT, $\Delta x'$,$\Delta y'$ approaching zero.

The value $S_0(x,y)\Delta x\Delta y\Delta T$ is the EBIV signal that would be obtained by raising the temperature of a region with an infinitesimal area $\Delta x\Delta y$ by ΔT. Thus, $S_0(x,y)$ furnishes information about the film properties solely for the point (x,y). Given S(x,y) over the entire film area, we can solve the integral eq. (4) for $S_0(x,y)$, which allows us to eliminate the influence of the temperature "tails" on the EBIV signal measured. To solve numerically the Fredholm integral eq. (4) of the first kind, we used a deconvolution method based on fast Fourier transforms. We applied the regularization method which minimizes the Tikhonov functional and determines the regularization parameter by the principle of generalized residual (Tikhonov and Arsenin, 1986).

Figure 2 illustrates the results of the treatment for a test structure: a meander-shaped series of YBaCuO microbridges prepared on a MgO substrate. The real

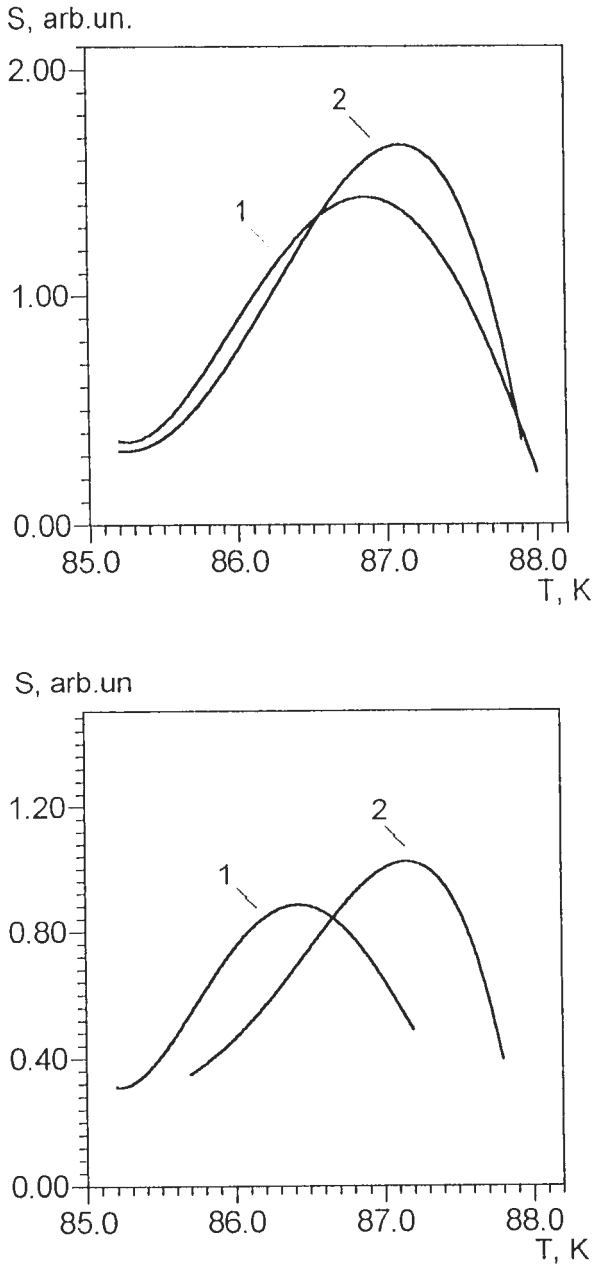

Figure 6. Local EBIV signals versus temperature for two neighboring points before (**a**) and after (**b**) the treatment eliminating the influence of the temperature "tails" on the EBIV signal. The distance between the points was about 5 μm.

---

geometry of the structure is shown in BSE mode (Fig. 2a). The EBIV images of the sample, before and after the treatment, are shown in digital form when bright and dark regions correspond to regions yielding EBIV signals exceeding, or being less than, 50% of the maximum signal, respectively. One can clearly see that a false EBIV signal (a signal enhanced in the center of the structure, due to the large contribution of surrounding

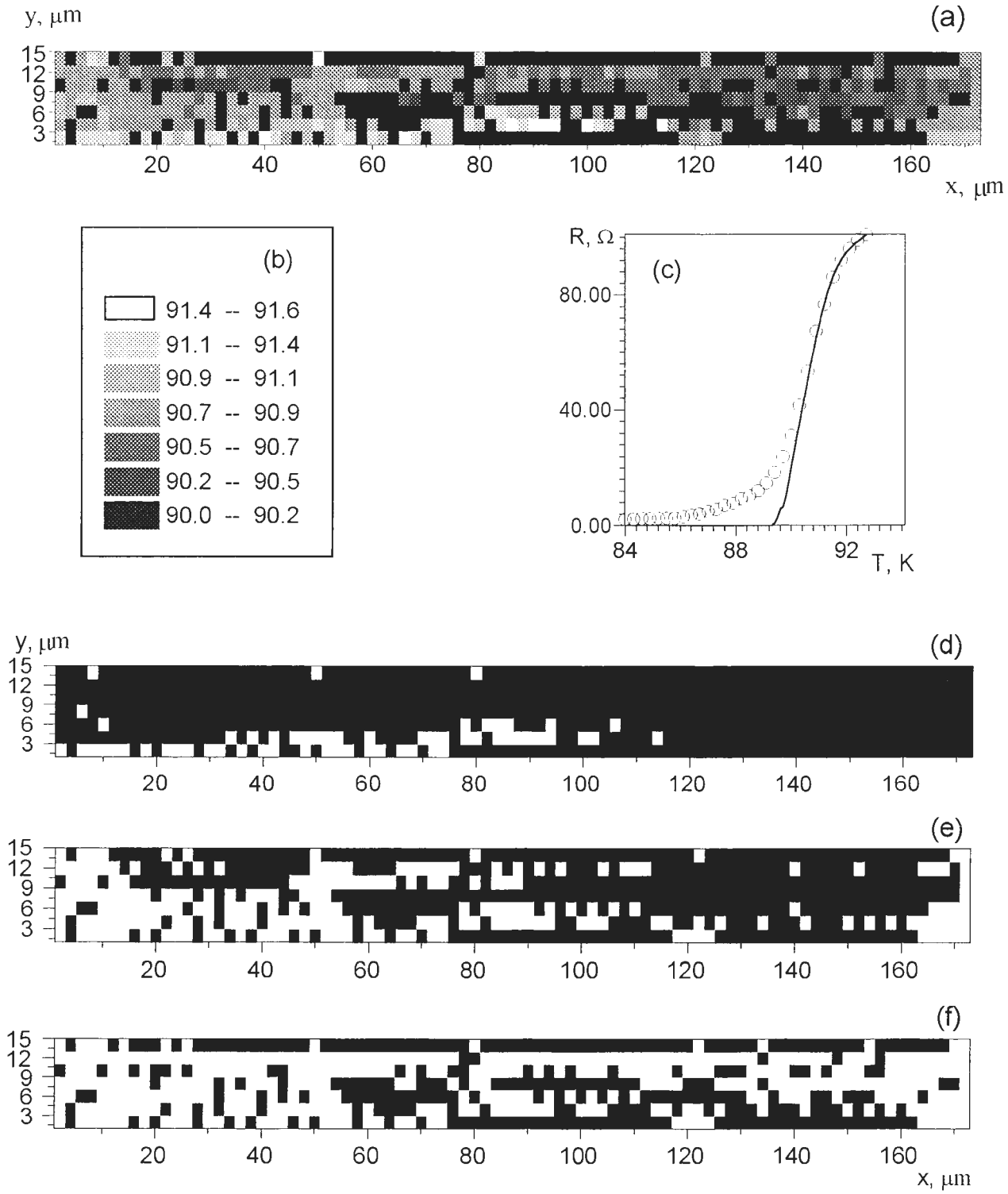

Figure 7 (a-f above; g and h on the facing page). Results of T_c-mapping for a YBaCuO/ $LaAlO_3$ film: a T_c-map (**a**) and the corresponding grey scale (**b**); experimental (circles) and calculated (solid line) R(T) dependencies (**c**); a two-dimensional distribution of superconducting (bright) and normal (dark) regions at T = 91.1K (**d**), 90.7K (**e**) and 90.3K (**f**); the current density distribution along the cross-sections at x = 90 μm (**g**) and x = 158 μm (**h**) at T = 91.1K (1), 90.7K (2) and 90.3K (3).

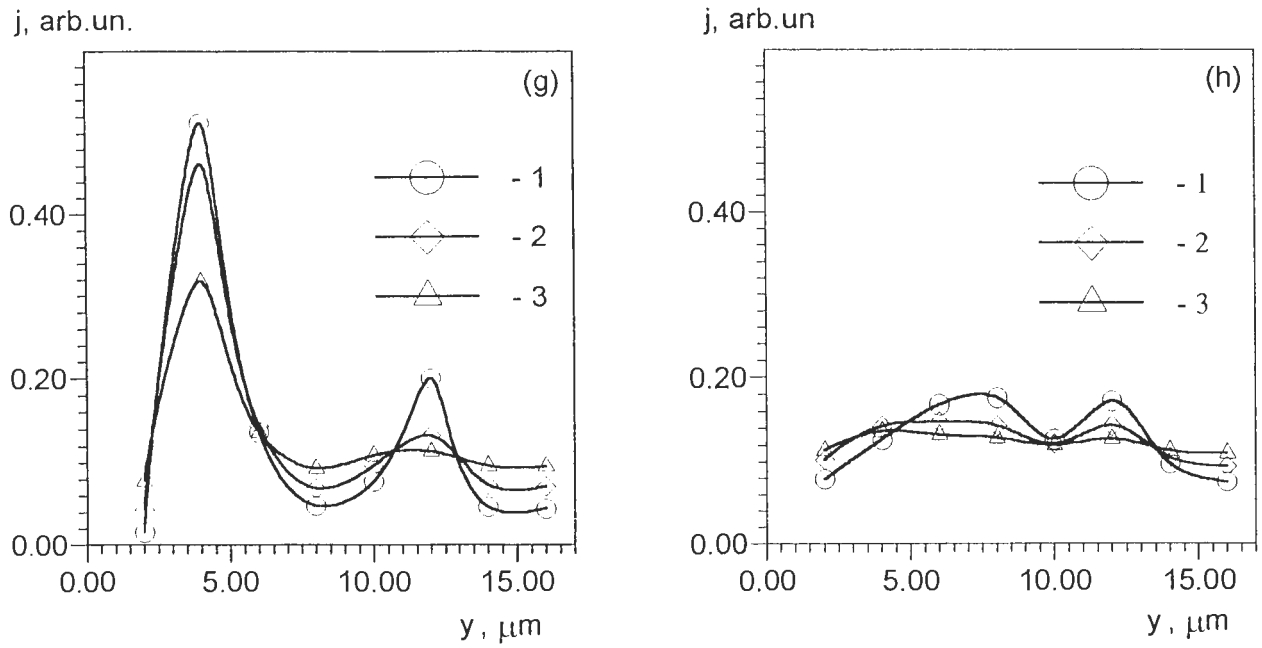

Figure 7 (see legend on the facing page).

regions) present in the original image (Fig. 2b) is eliminated after the treatment (Fig. 2c).

Influence of absorbed current

The absorbed charge is well known to be carried to earth by a flow of electrons through a sample subjected to electron beam irradiation. Thus, the observed EBIV signal consists not only of the component associated with a local change of superconducting parameters of a HTSC film, but of a component caused by the absorbed current as well. At given temperature, this component depends on the coordinate x aligned with the long side of a microbridge and on the value of the absorbed current:

$$S_{ab}(x) = S(x)\,|_{j=0} = I_{ab}(x)_x \int^{l} \{\rho(\xi)(d\xi/\sigma(\xi))\}, \quad (5)$$

where I_{ab} is the absorbed current, l and σ are the length and the cross-sectional area of the microbridge, respectively. The absorbed current contributes significantly to the signal when thin, inhomogeneous, or high-resistivity films or device structures {bolometers, superconducting quantum interference devices (SQUIDs), etc.} are studied or the measurements are done at very low bias current densities. Furthermore, $S_{ab}(x)$ is a non-linear function of temperature. This may lead to a modification of the S(T) curve shape and, consequently, to errors in local measurements of T_c and ΔT_c.

The absorbed current effect is taken into account by recording the EBIV signals $S_+(T)$ and $S_-(T)$ under forward and reverse bias, respectively. Then the true signal S(T) can be obtained as:

$$S(T) = (1/2)\,\{S_+(T) + S_-(T)\} \quad (6)$$

Figure 5 presents experimental temperature dependencies of the EBIV signals $S_+(T)$, $S_-(T)$, and S(T) obtained on a meander-shaped series YBaCuO/MgO microbridges, their total length being about 2.5 mm. One can see that the maxima of the $S_+(T)$ and $S_-(T)$ curves are significantly shifted in temperature from the maximum of the S(T) curve. The sign of the shift is determined by the bias polarity while its magnitude depends on coordinate x. This shift leads to an error in the measured value of T_c. For the EBIV signals of Figure 5 this error was about 0.8K.

T_c-Mapping

Procedure of T_c-mapping

The two stages of T_c-mapping procedure are:

(1) Experimental measurement of the EBIV spatial distribution is carried out over the temperature range of the superconducting transition. The measurements are performed at fixed points. A two-dimensional array of these points is set to fit the geometry of the sample investigated. The distance between neighboring points is chosen in accordance with the electron range R_e. At given temperature, the surface of the HTSC film is sequentially scanned, point to point by the electron beam. For every point, the EBIV signals are measured both under forward and reverse bias, followed by the calculation of the true signal (see the previous section). As a result, a three-dimensional array, S(T,x,y), is derived.

(2) The obtained data are treated by the numerical deconvolution method to eliminate the influence of the temperature "tails" on the measured EBIV signal (see **Influence of the temperature "tails"**). In addition to increasing the spatial resolution in EBIV mode, the treatment allows the superconducting parameters to be measured more correctly at each point. Figure 6 shows local S(T) dependencies for two neighboring points before and after the treatment. It can be clearly seen that the initial EBIV curves almost coincide, while after the treatment, they substantially differ in shape and position of the maximum. Finally, using the deconvoluted array $S_0(T,x,y)$, one can derive the spatial distribution of critical temperature, namely the T_c-map. For each point, the values of T_c and ΔT_c are estimated as the position of the maximum and the full width at half maximum (FWHM) of the appropriate $S_0(T)$ curve, respectively. It should be taken into account that the position of the $S_0(T)$ maximum is shifted from T_c by the value $\Delta T/2$. At $\Delta T << \Delta T_c$, this shift is negligible and the superconducting parameters can be directly found from the $S_0(T)$ curve (Koelle *et al.*, 1990). Otherwise, the value of ΔT can be determined by fitting a $S_{int}(T)$ curve calculated from the integral R(T) dependence of a sample to a $\overline{S(T)}$ curve averaged over the entire sample area (Konnikov *et al.*, 1992).

Applications of the T_c-map

Once the T_c-map is obtained, the spatial distribution of the current density over the film can be calculated. Along with the T_c-map, this information is also important for an unambiguous interpretation of experimental results obtained by standard four probe techniques.

In our calculations, we use the model of resistance network (Kirckpatrick, 1973). A microbridge is divided into fragments whose size is limited by the spatial resolution of the EBIV method. Given the T_c-map of a film, the values of T_c and ΔT_c are known for each fragment (x,y). For simplicity, we assume that each fragment has a definite resistance r(x,y) which depends on the temperature T and is given by

$$r(x,y) = 0, \text{ when } T < T_c^{off};$$

or

$$r(x,y) = \{T - T_c(x,y) + \Delta T_c(x,y)\} / 2\Delta T_c(x,y), \quad \text{for } T_c^{off} < T < T_c^{on};$$

or

$$r(x,y) = 1, \text{ for } T > T_c^{on}, \qquad (7)$$

where

$$T_c^{off} = T_c(x,y) - \Delta T_c(x,y)$$

and

$$T_c^{on} = T_c(x,y) + \Delta T_c(x,y)$$

Furthermore, it is assumed that the resistances are connected in a rectangular two-dimensional network in such a way that the resistance of the bond between the nodes (x_1,y_1) and (x_2,y_2) is equal to $\{r(x_1,y_1)+r(x_2,y_2)\}/2$. At given temperature, one can calculate the current passing through each bond in the network by solving a set of Kirchhoff's equations for the potentials $\phi(x,y)$ at each node. Needless to say, the total resistance R of the network can be calculated in this way. Comparison of a calculated R(T) curve with the experimental one can be used to control the validity of the T_c-map.

The results of T_c-mapping for a $YBaCuO/LaAlO_3$ film whose c-axis lies in the film plane and is perpendicular to the direction of the microbridge are presented in Figure 7. The T_c-map clearly demonstrates that the critical temperature varies over the microbridge from 90.0K to 92.0K (Fig. 7a). The critical temperatures were measured with an accuracy of 0.2K, the spatial resolution being 2 μm. The values of T_c for black regions in Figure 7 appear to be lower than T_c^{off} for the film as a whole. For the low-temperature part of the superconducting transition region ($T < T_c^{off}$), the film resistance is only determined by weak links formed at scratches on the substrate. This leads to a substantial discrepancy between the R(T) calculated using the T_c-map and the experimental dependence for $T < T_c^{off}$ (Fig. 7c). Thus, one can estimate temperature intervals where the transport properties of the film are controlled either by the spatial distribution of volume fragments with different T_c or by that of weak links with different j_c values.

Using the T_c-map, the spatial distribution of superconducting and normal regions can be readily obtained at a given temperature. Figures 7d, 7e, and 7f present patterns of such a distribution in the film for three different temperatures. The patterns show stages of superconducting cluster formation and present evidence that the transition from the non-superconducting to the superconducting state occurs across the whole microbridge via the percolation mechanism. The current lines are concentrated in the superconducting regions of the film. That is why the current density distribution is very inhomogeneous over the cross-section at x = 90 μm (Fig. 7g) containing regions with strongly different T_c, while for the cross-section at x = 158 μm (Fig. 7h), it is almost unchanged throughout the transition.

One more application of the T_c-map is direct determination of the distribution function $f(T_c)$ of critical temperatures. This function shows the fraction of film fragments with given T_c where

$$\int_{-\infty}^{+\infty} f(T_c)dT_c = 1.$$

It is of special interest and can be used to explain the experimental temperature dependencies of paraconductivity, thermopower, magnetoconductivity and flicker noise

Table 1. Preparation of sample.

	Sample A	Sample B	Sample C	Sample D
substrate	(001) MgO		(110) $LaAlO_3$	
film structure	epitaxial	granular	granular	
film orientation	c-axis oriented		[100]-axis oriented	
surface morphology	smooth	rough, with pinholes and inclusions	parallel single-crystal grains	
thickness (nm)	240	260	320	320
orientation of long side of the microbridge	-	-	perpendicular to c-axis	parallel to c-axis
$\sqrt{\left\langle \left(\frac{\Delta c}{c}\right)^2 \right\rangle}^{(*)}$ (10^{-3})	0.91	0.94	-	-
T_c (K)	90.2	87.1	89.9	89.9
ΔT_c (K)	0.6	2.6	1.5	3.9
ρ at 100 K ($\mu\Omega$cm)	90	140	110	11470

*Internal microstrain fluctuation was measured by triple crystal X-ray diffractometry (Gong *et al.*, 1994).

(Bobyl *et al.*, 1995). In **Water modification of T_c-distribution function**, this function is used to describe the evolution of an ensemble of fragments during the water-initiated modification. The distribution function $f(T_c)$ can be also derived from the R(T) dependence using the percolation approach (Forgacs *et al.*, 1991; Bobyl *et al.*, 1995). However, this method is very approximate since, first, the percolation approach is applicable only in a narrow temperature interval near the percolation threshold and, second, the corresponding critical index may be assigned arbitrarily.

Samples and Experimental Apparatus

Superconducting YBaCuO films were prepared by DC magnetron sputtering of a ceramic stoichiometric target. The films were grown at a rate of about 2 nm/min at T = 680K in a gaseous mixture of argon and oxygen. Subsequent heat treatment at T = 500K for 20 minutes in pure oxygen at a pressure of about 1 atm and cooling for 1 hour resulted in a high oxygen saturation of the YBaCuO lattice (Karmanenko *et al.*, 1993). The film thickness was in the range 200-400 nm.

Preliminary characterization by X-ray diffractometry has shown the presence of only (00m) reflections for films grown on (100) MgO substrates, which confirms the (100)-orientation of the films, whereas in the case of films grown on (110) $LaAlO_3$ substrates, only (kl0) reflections have been observed. Investigation of the anisotropy of polarization-dependent Raman spectra in YBaCuO/$LaAlO_3$ films confirms their [110]-orientation.

Microbridges were formed on the films by a standard photolithographic procedure. The typical test structure was composed of microbridges with different geometrical parameters and orientation as well as of a meander-shaped series of microbridges. The microbridges were 20 to 60 μm wide and 500 μm long.

Properties and characteristics of typical samples studied in this paper are listed in Table 1.

Measurements were carried out with an automated scanning electron microscope, CamScan Series 4-88 DV100 (Cambridge Scanning Company Limited, Cambridge, U.K.) equipped with a sample cooling system ITC4 (Oxford Instruments Limited, Oxford, U.K.) (the temperature could be maintained to within 0.1K in the range 77-300K) and a low-noise amplifier for voltage signals. The bias current I_{tot} was varied from 0.2 to 2.0 mA, so that the transition behavior will not be affected by its value. To extract the local EBIV signal, lock-in detection was used with a beam-modulation frequency of 1 kHz. The electron beam parameters were the following: the accelerating voltage was 10 kV, and the beam current was 10^{-8} A.

Results and Discussion

Preliminary LTSEM study

In the following, T_c-mapping is demonstrated to be a powerful tool for studying the process of water-initiated modification of thin YBaCuO films.

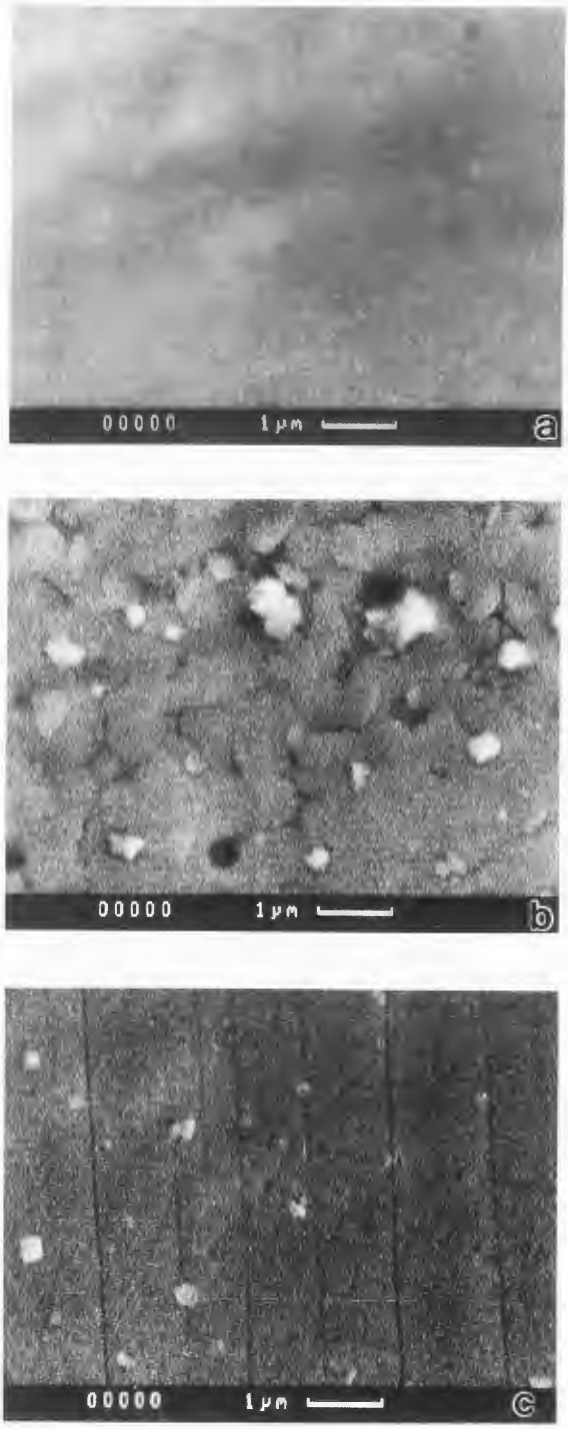

Figure 8. Surface morphology of YBaCuO/MgO (**a**, **b**) and YBaCuO/$LaAlO_3$ (**c**) films. Bars = 1 μm.

The films investigated were divided into four groups; typical samples for each of these are denoted by A, B, C, D (see Table 1). Samples A and B were formed on c-oriented YBaCuO films grown on MgO substrates. The films were grown under the same technological conditions, but on the substrates of different

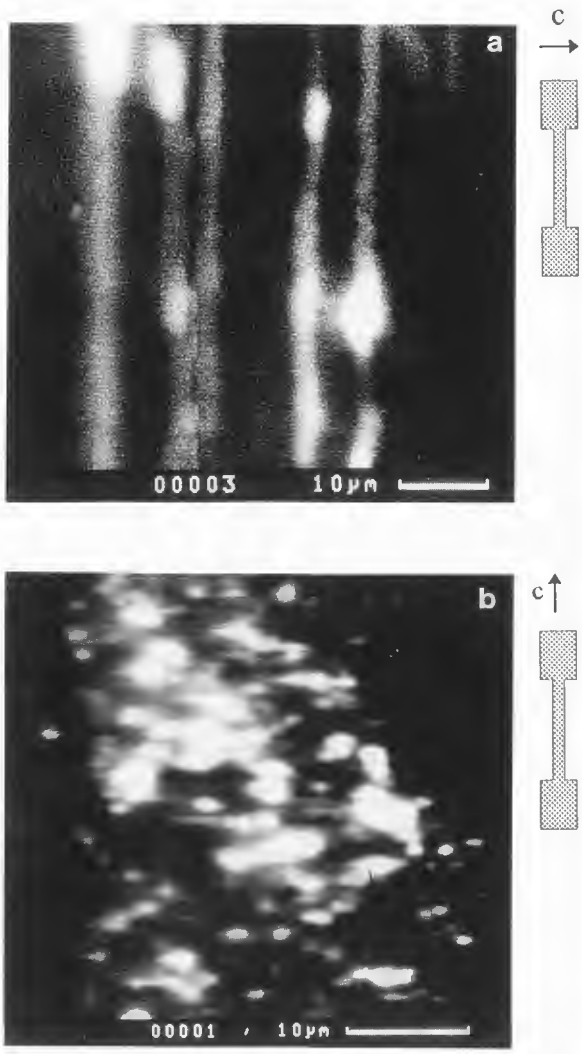

Figure 9. EBIV images of sample C (**a**) and D (**b**) at T = 87K. The c-axis direction relative to the microbridge is shown schematically at right. Bars = 10 μm.

---

quality. The substrate surface for sample B had defects known as "etching holes", while the substrate surface for sample A was free of them. The morphology of the films was also different. Sample A was smooth, while in sample B grains, inclusions and pinholes were observed (Figs. 8a and 8b).

Samples C and D were formed from a [110]-oriented film grown on a vicinal surface of an $LaAlO_3$ substrate. It is well known that YBaCuO films exhibit very strong anisotropy: growth rate and conductivity are far less in the c-direction than in the (a,b)-plane (Takenaka *et al.*, 1994). Therefore, in the case, when the c-axis lies in the film plane, the film consists of almost monocrystalline domains in the form of long narrow stripes directed normal to c-axis. In the films studied, the stripe width was about 1 μm (Fig. 8c).

The only difference between samples C and D is

that the long side of the microbridge is perpendicular to the c-axis in the former and aligned with it in the latter. Figure 9 shows EBIV images of the samples at a temperature $T < T_c^{off}$. In this case, the EBIV image represents the current distribution across the sample (see **The fundamentals of LTSEM**). Because of conductivity anisotropy and the presence of boundaries between neighboring stripes, current percolation along c-axis is severely limited. Therefore, the current lines in sample C never cross the stripe boundaries, and the EBIV image is a sequence of bright lines directed along the microbridge and associated with stripes in which current lines are concentrated (Fig. 9a). Different stripes have different current densities, depending on the presence of defects in each stripe. As one can see, the distance between the stripes with high current density may be as large as 10 μm. In sample D, current crosses each boundary at the points where neighboring stripes have the best electrical contact. Since the current is concentrated at these points (weak links), they correspond to bright regions on the EBIV image (Fig. 9b). It can be seen that each boundary contains one or more weak links. The EBIV images of separate weak links have an elliptical shape, owing to the anisotropy of thermal conductivity in YBaCuO (Gross and Koelle, 1994). This anisotropy should be taken into account in T_c-mapping. It is worth noting that in sample D, the real length to be passed by the current far exceeds the bridge length and the total resistance and critical current of the bridge as a whole are strongly determined by the properties of weak links.

The granularity of the HTSC films implies that weak links between grains have a profound effect on their resistance, especially in the low-temperature part of the transition region (Koelle *et al.*, 1990; Gaevski *et al.*, 1994). It is rather difficult to determine the role of weak links when analyzing the R(T) dependence measured for the microbridge as a whole, because its shape can be affected not only by micro- but also by macroinhomogeneities. For example, the low-temperature tail of the transition curve can be accounted for by the cracks, photolitographically induced defects and T_c-macroinhomogeneities. The use of local temperature dependencies of EBIV, S(T), allows one to eliminate the problem of influence of such inhomogeneities (Bobyl *et al.*, 1995). For samples C and D formed on the same granular film on $LaAlO_3$, dependencies of this kind have low-temperature tails, which proves the presence of weak links in the film (Fig. 10). Furthermore, sample D with the highest concentration of weak links in the path of current has the broadest low-temperature part of the local transition region. By contrast, the local S(T) dependencies for sample A are found to drop abruptly at low temperatures, which indicates the absence of weak

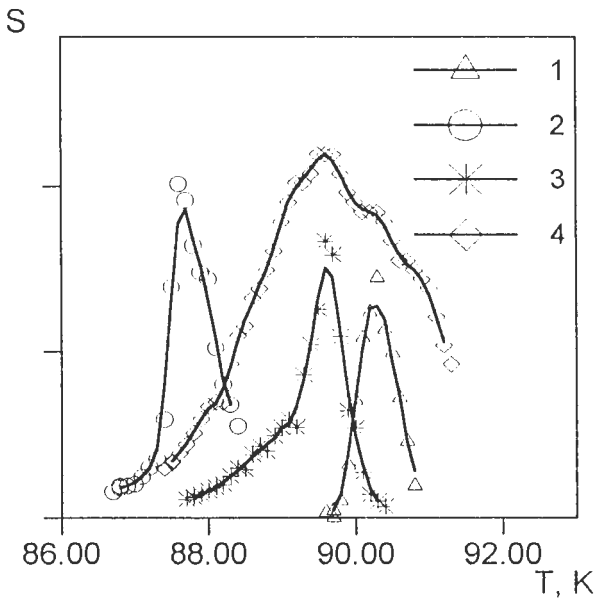

Figure 10. Local S(T) curves for samples A (**1**), B (**2**), C (**3**), and D (**4**). The solid curves are drawn through the experimental points as guides to the eye.

---

links (Fig. 10). Comparison of X-ray, Raman and SEM data (Fig. 8a) suggests that sample A is epitaxial. For sample B, the S(T) curve shows a low-temperature tail (Fig. 10); the EBIV data and the SE image (Fig. 8b) are indicative of the granular structure of sample B.

To select microbridges for water-initiated modification experiments, we used LTSEM in much the same way as it was done for a series array of tunnel junctions (Huebener, 1987). Viewing the EBIV images of an array of parallel-connected microbridges enables the faulty element to be revealed together with the element exhibiting the best parameters. The results of such investigations for four parallel-connected microbridges are presented in Figure 11. Figure 11b shows the S(T) curves for the microbridges. Each of the curves is obtained by averaging the EBIV over the entire area of the corresponding microbridge. It can be established from the S(T) dependence of microbridge #3 that it does not undergo superconducting transition, while microbridge #2 exhibits the highest S(T) peak, which is indicative of its low resistance in normal phase. The transition curves for each of four microbridges obtained after separation of the microbridge contacts by laser ablation are also shown in Figure 11c. These curves agree fairly well with predictions made on the basis of the EBIV studies. There peak position and FWHM of the S(T) are strongly correlated with T_c and ΔT_c, respectively. The procedure we have developed allows one to make a correct choice of samples to be studied. In this case, no repeated thermocycling of samples is necessary.

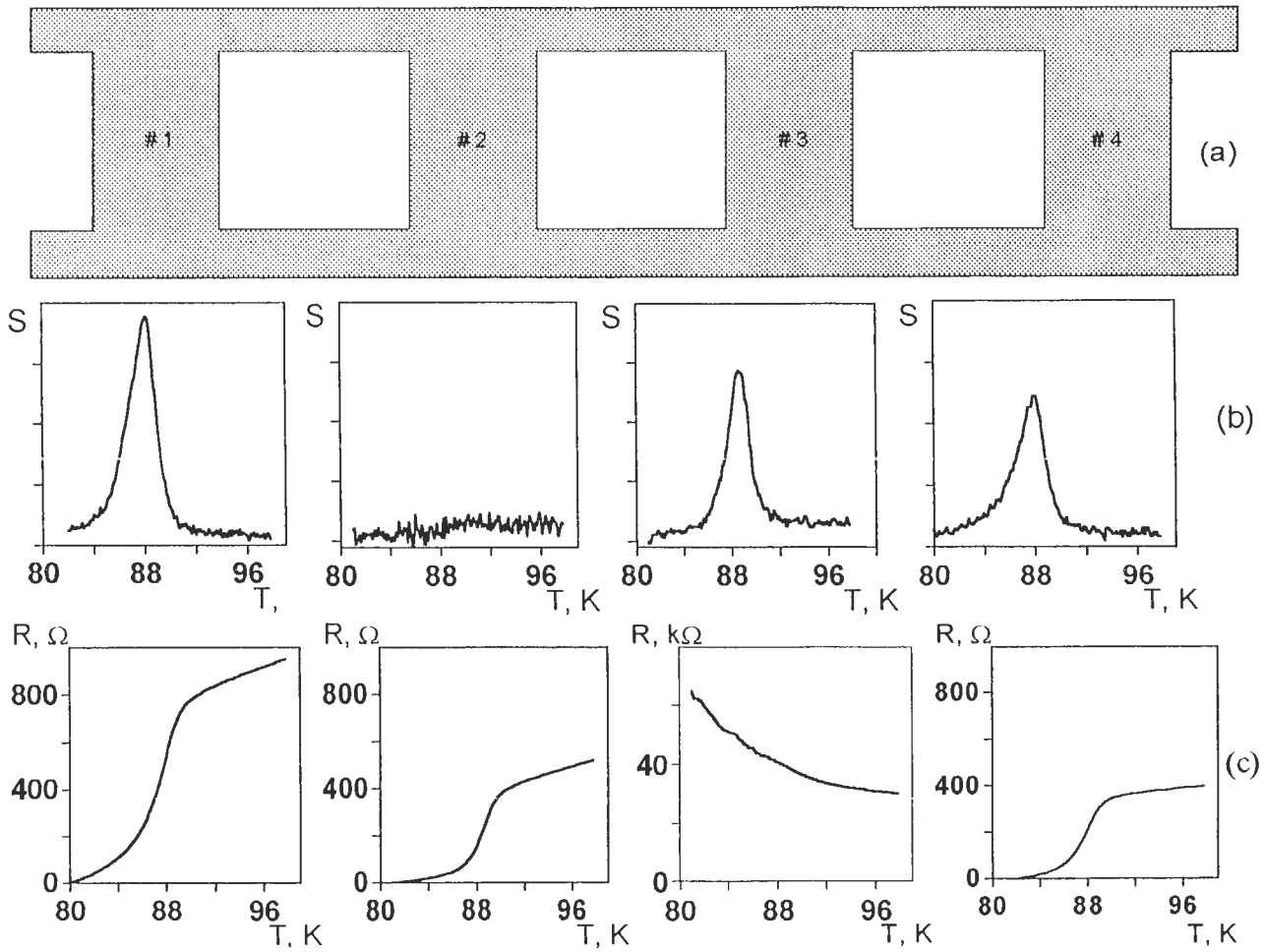

Figure 11. Schematic configuration (**a**) and S(T) curves (**b**) for four parallel-connected microbridges and the R(T) curves (**c**) obtained after separation of the microbridge contacts by laser ablation.

Water-initiated modification of the T_c -distribution function

Water-initiated degradation of HTSC materials has been widely investigated under various conditions. A number of effects have been observed: (**a**) a change of T_c and the shape of the transition curve (Kishida *et al.*, 1988), (**b**) surface corrosion (Jandl *et al.*, 1989), (**c**) formation of an amorphous surface layer and of planar defects (Zhao and Myhra, 1994) and (**d**) chemical decomposition (Jin *et al.*, 1989; Salvador *et al.*, 1989). It should be noted that most of these investigations have been carried out on ceramics or powder specimens. In the present work, the water-initiated degradation of thin YBaCuO films is studied and the local LTSEM technique is used, to our knowledge, for the first time for investigating this process.

The samples were stored for a specified time in distilled water at 300K. Water-initiated modification was observed for the R(T) transition curve, the EBIV image, the distribution function $f(T_c)$ and the T_c-ensemble of film fragments.

The first point to be noticed is that storage in water enhances the inhomogeneity of the film. The EBIV images shown in Figure 12 demonstrate a dramatic increase in the extent of inhomogeneity induced by water in the spatial current density distribution. This effect originates from the significant T_c-shift occurring in some fragments of the film, as a result, the global superconducting transition is broadened, whereas the width of the local transition region shows no substantial increase.

Figure 13 illustrates the water-initiated modification of the T_c-distribution functions for samples A, B and C having different morphology and orientation; clearly, in the first stage of modification, the average critical temperature tends to increase. In the second stage of modification (namely, the degradation stage), the average T_c starts to decrease while the distribution function becomes wider. This behavior is most pronounced for sample A,

which has the narrowest T_c-distribution. The rise in T_c for a YBaCuO ceramic has been observed by Kishida *et al.* (1988). This effect is of universal nature, being observed upon oxygen annealing (Janod *et al.*, 1993), various dopings (Fisher *et al.*, 1993), and irradiation (Shiraishi, 1989). It is common knowledge that the physical properties of the $YBa_2Cu_3O_{7-x}$ compound depend strongly on the oxygen deficiency, x. It has been shown that the critical temperature first increases with x and then starts to decrease (for $x > 0.07$). Moreover, the $T_c(x)$ dependence at small x values can be described by a parabola $T_c = ax + bx + c$ (Janod *et al.*, 1993). It may be assumed that the change in T_c during water-initiated modification of HTSC films also results from the decrease in oxygen content.

Thanks to the developed technique of T_c-mapping, we have a possibility to observe a water-induced shift of local critical temperature, Δ_w, at any point of the sample. This information can be used to estimate the value of the decrease in oxygen content, Δx. In our estimation, Δx is the same for all the points. Figure 14 shows the correlation between the initial T_c and the shift of T_c induced by storage of sample B in water for 1000 seconds. Each point on the plot is obtained by averaging T_c over the film fragments with the same Δ_w. If the water-induced shift Δx were uniform throughout the sample, the $T_c(\Delta_w)$-curve would also have a parabolic form, $T_c = A\Delta_w + B\Delta_w + C$, where $A = 1/(4a\Delta x)$. To check our hypothesis, we analyzed the coefficients of the parabola that best fits the data obtained. Taking into account the fact that $\Delta x_{13} = \Delta x_{12} + \Delta x_{23}$, where indexes define the initial and the final state of the process [before the storage in water(1), after 1000 seconds in water (2), after 2000 seconds in water (3)], one can check the validity of the corresponding relation between the coefficients of the parabola. This relation appeared to be true with an accuracy of about 15%.

To describe the rate of water-initiated modification of the films, we used the ratio $\Delta x/\Delta t$, where Δt is the storage time. The values of Δt and the calculated values of Δx and $\Delta x/\Delta t$ for samples A, B and C are listed in Table 2. In calculations, we used the value of the coefficient "a" taken from Janod *et al.* (1993). As can be seen from Table 2, the modification rate depends strongly on the film orientation (see data for samples A and C). Meanwhile, the presence of grains and some defects on the surface of a c-axis-oriented film leads to an increase in the modification rate by only a factor of two (see data for samples A and B).

At first glance, it would be reasonable to relate the observed dependence of the modification rate on the film orientation to the anisotropy of oxygen diffusion in YBaCuO. The diffusion was found to be extremely anisotropic $D_{ab} > 10^4 - 10^6 D_c$ (Rothman *et al.*, 1991),

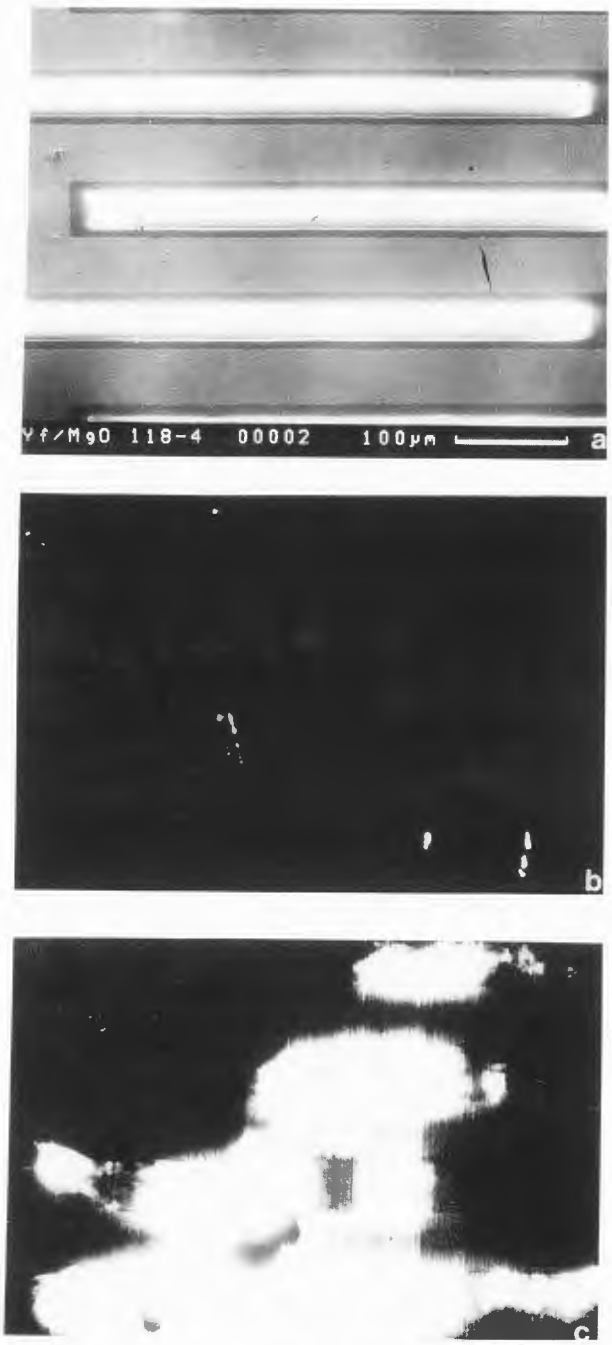

Figure 12. Images of sample A in SE mode (**a**) and in EBIV mode before (**b**) and after (**c**) storage in water for 4000 seconds.

Table 2. Water-initiated modification rate.

	Sample A	Sample B	Sample C
Δx	0.09	0.08	0.17
Δt, sec.	2000	1000	100
$\Delta x/\Delta t$ arb. units	1	2	40

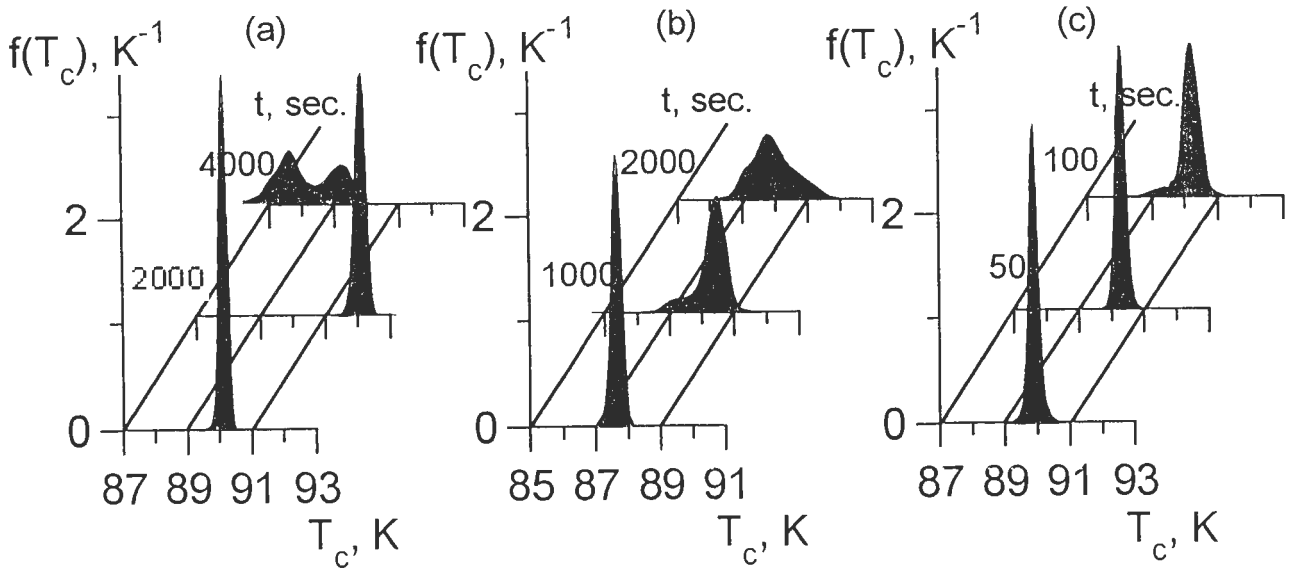

Figure 13. Results of water-initiated modification of the T_c-distribution function for samples A (**a**), B (**b**) and C (**c**). Here t is the storage time of a sample in water. The t-axis scales are different for each of the samples.

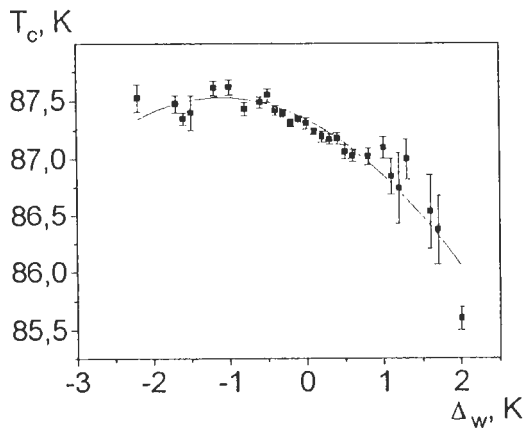

Figure 14. Correlation between the initial T_c and the shift of T_c induced by storage of sample B in water for 1000 seconds. Each point on the plot is obtained by averaging T_c over the film fragments with the same Δ_w. The solid line is the parabola that best fits the data obtained.

$D_{ab} > 10^5 D_c$ (Tsukui *et al.*, 1991), where D_{ab} and D_c are the oxygen diffusion coefficients in (a,b)-plane and along the c-axis, respectively.

Assuming that the decrease in the oxygen content in the film is due to oxygen diffusion towards the surface and the value of $\Delta x/\Delta t$ is proportional to the oxygen diffusion coefficient, we obtain $D_{ab}/D_c = 40$. This value is in strong disagreement with the above mentioned experimental results and indicates the existence of another diffusion mechanism that does not involve oxygen. The most plausible mechanism discussed (Chudnovski *et al.*, 1990) is penetration of hydrogen which is actively generated when YBaCuO reacts with water at T = 400K. It should be noted that there is a possibility of hydrogen tunneling through potential barriers that may substantially increase its diffusion coefficient along the c-axis. It has been shown that hydrogen neutralizes charge carriers in YBaCuO thereby reducing the carrier concentration (Dortmann *et al.*, 1994). Hence, hydrogenation of YBaCuO increases the resistivity and changes T_c in a similar manner as the decrease in oxygen content. The quantity Δx may be considered as an effective change of oxygen deficiency, since the number of oxygen atoms that actually take part in superconductivity decreases as a result of hydrogenation.

Examination of [110]-oriented films shows that the modification rates of the temperature dependencies of resistance R(T) were substantially different for microbridges oriented normal to the c-axis and along the c-axis (see curves 1, 2 in Figures 15a and 15b). The shape of the R(T) curve and the value of T_c for sample C were almost unchanged after storage of the sample in water for Δt = 100 seconds. By contrast, in sample D, the temperature dependence of resistance in the normal state and the values of T_c and ΔT_c changed dramatically. This is because the [110]-oriented film consists of an array of grains extended in one direction. As shown in the previous section, such a film structure leads to different patterns of current flow in samples C and D. In sample D, the grain boundaries produce a far more pronounced effect on the characteristics we measured {R(T), S(T), T_c-distribution} than in sample C. The increased modification rate of R(T) for sample D seems to be associated with the grain boundary modification which proceeds faster than the modification of the inner

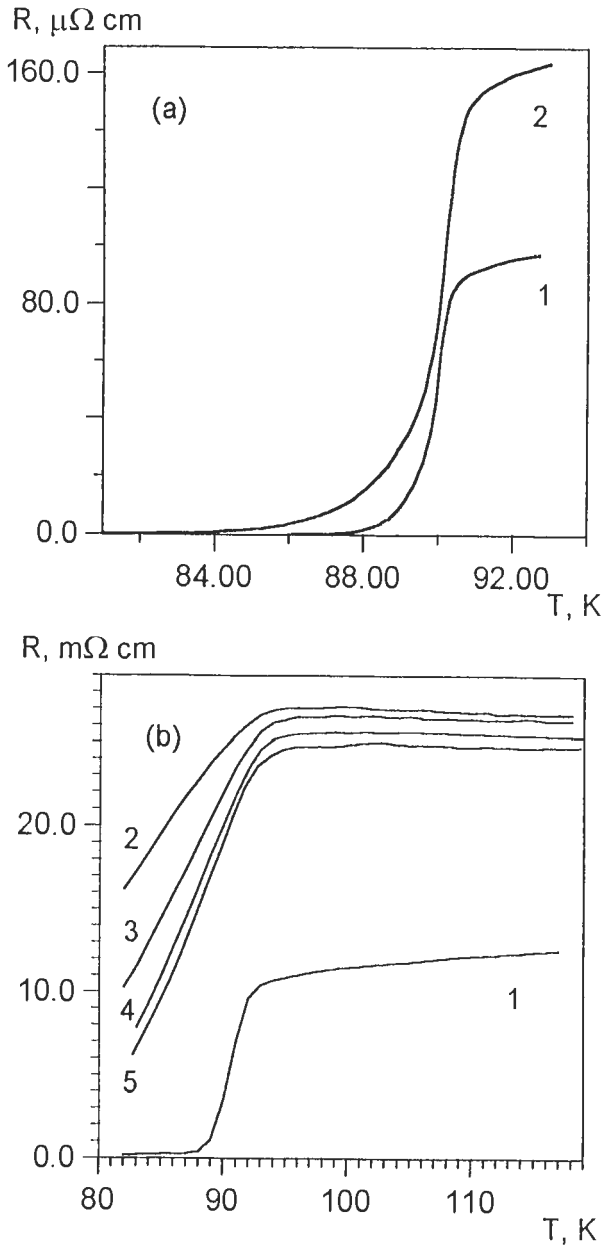

Figure 15. R(T) curves for samples C (**a**) and D (**b**) before (**1**) and after storage of the samples in water for 100 seconds (**2**), and after sequential storage in vacuum for 1.5 days (**3**), in atmosphere for 2 days (**4**), and finally in vacuum for 3 days (**5**).

---

parts of the grains. The information on water-initiated modification of sample C derived from T_c-mapping results refers to the inner parts of the grains. Thus, it is the use of data obtained for sample C, rather than for sample D, that makes the above analysis of the effect of film orientation on the modification rate correct.

It has been found that the effect of exposure to water is reversible to some extent. Figure 15b presents the results of R(T) measurements carried out for the water-modified sample D at intervals. It will be seen that the rate of relaxation does not depend on the presence of ambient oxygen. This fact confirms the above-mentioned idea that YBaCuO films are hydrogenated during water-initiated modification.

Acknowledgments

The work was supported by ISF Grant #R3J000 and Russian National Program Project #94048. The authors would like to thank R.N. Kutt and V.Yu. Davydov for X-ray and Raman measurements, and S.F. Karmanenko for providing high-quality samples.

References

Barns RL, Laudise RA (1987) Stability of superconducting $YBa_2Cu_3O_7$ in the presence of water. Appl Phys Lett **51**: 1373-1375.

Bobyl AV, Gaevski ME, Khrebtov IA, Konnikov SG, Shantsev DV, Solov'ev VA, Suris RA, Tkachenko AD (1995) Resistance flicker noise and current percolation in c-oriented $YBa_2Cu_3O_{7-x}$ films in the vicinity of T_c. Physica C **247**: 7-33.

Butterweck HJ (1975) Noise voltages of bulk resistors due to random fluctuations of conductivity. Philips Res Repts **30**: 316-321.

Chudnovski FA, Baikov YM, Egorov EA, Zhizhenkov VV, Kozlova IR, Shalkova EK (1990) Hydrogen in $Ba_2YCu_3O_{7-y}$ ceramic. Sverhprovodimost **3**: 99-108 (in Russian).

Clem JR, Huebener RP (1980) Application of low-temperature scanning electron microscopy to superconductors. J Appl Phys **51**: 2764-2773.

Dortmann G, Erxmeyer J, Blasser S, Steiger J, Paatsch T, Weidinger A, Karl H, Stritzker B (1994) Hydrogenation of thin Y-Ba-Cu-O films: Electrical transport and structure properties of $YBa_2Cu_3O_7$ and $YBa_2Cu_3O_8$. Phys Rev B **49**: 600-606.

Fisher B, Genossar J, Patlagan L, Reisner GM (1993) Hole filling in a narrow conduction band in $YBa_2Cu_{3-x}Co_xO_{7-\delta}$ ($x < 0.3$). Phys Rev B **48**: 16056-16060.

Forgacs G, Schulman LS, Kiss LB, Svedlindh P, Lundgren L (1991) Method for determining the distribution of Josephson coupling energies in high-T superconductors. Physica C **177**: 67-72.

Gaevski ME, Demidov DM, Denisov DV, Konnikov SG, Kulagina MM, Smol'skii OV, Chalyi VP (1994) Mesa structures with a high-temperature superconducting layer of YBaCuO. Tech Phys Lett **20**: 21-23.

Gong JP, Kawasaki M, Fujito K, Tsuchiya R, Yoshimoto M, Koinuma H (1994) Investigation of precipitate formation on laser-ablated $YBa_2Cu_3O_{7-\delta}$ thin films. Phys Rev B **50**: 3280-3287.

Gross R, Koelle D (1994) Low-temperature scanning electron microscopy. Rep Prog Phys **57**: 651-736.

Gross R, Hartmann M, Hipler K, Huebener RP, Kober F, Koelle D (1989a) Spatial resolution limit for the investigation of high-T_c films by low temperature scanning electron microscopy. IEEE Trans Mag **25**: 2250-2253.

Gross R, Hipler K, Mannhart J, Huebener RP, Chaudhari P, Dimos D, Tsuei CC, Schubert J, Poppe U (1989b) Spatial imaging of the critical current density in epitaxial $YBa_2Cu_3O_7$ films. Appl Phys Lett **55**: 2132-2134.

Huebener RP (1987) Scanning electron microscopy at very low temperature. In: Advances in Electronics and Electron Physics, Vol. 70. Hawkes PW (ed.). Academic Press, New York. pp. 1-78.

Huebener RP, Gross R, Bosch J (1988) Low-temperature scanning electron microscopy for studying inhomogeneities in thin-film high-T_c-superconductors. Z Phys B: Condensed Matter **70**: 425-430.

Jandl S, Banville M, Dufour P, Gagnon R (1989) The influence of the quasi-two-dimensional character of carriers and corrosion effects on mid-infrared reflectance of $YBa_2Cu_3O_{7-x}$. Solid State Commun **70**: 337-340.

Janod E, Junod A, Graf T, Wang KQ, Triscone G, Muller J (1993) Split superconducting transitions in the specific heat and magnetic susceptibility of $YBa_2Cu_3O_x$ versus oxygen content. Physica C **216**: 129-139.

Jin SG, Liu LG, Zhu ZZ, Huang YL (1989) Water reaction of superconducting $YBa_2Cu_3O_7$ at 0C and its protection from water corrosion at 100C. Solid State Commun **69**: 179-182.

Karmanenko SF, Davydov VY, Belousov MV, Chakalov RA, Dzjuba GO, Il'in RN, Kozyrev AB, Likholetov YV, Njakshev KF, Serencov IT, Vendic OG (1993) The formation of two-layered YBaCuO superconducting films and their microwave surface resistance. Supercond Sci Technol **6**: 23-29.

Kirckpatrick S (1973) Percolation and conduction. Rev Mod Phys **45**: 574-588.

Kishida S, Tokutaka H, Nishimori K, Ishihara N, Watanabe Y, Noishiki Y, Yamamoto T (1988) Effects of water on the resistance-temperature characteristics of $YBa_2Cu_3O_{7-y}$ oxides. Jpn J Appl Phys **27**: L1616-L1619.

Koelle D, Kober F, Hartmann M, Gross R, Huebener RP, Roas B, Schultz L, Saemann-Ischenko G (1990) Spatially resolved measurements of the resistive transition in epitaxial YBaCuO-films. Physica C **167**: 79-88.

Konnikov SG, Solov'ev SA, Solov'ev VA, Gaevski ME (1992) Determination of the local parameters (T_c, ΔT_c) in high-T_c superconducting films. Pis'ma Zh Tekh Fiz **18**: 20-23 (or Sov Tech Phys Lett **18**: 696-697).

Mannhart J, Gross R, Hipler K, Huebener RP, Tsuei CC, Dimos D, Chaudhari P (1989) Spatially resolved observation of supercurrents across grain boundaries in YBaCuO films. Science **245**: 839-841.

Nishihara H, Nishida N, Takabatake T, Kishio K, Ohtomo A, Hayashi K, Ishikawa M, Nakazawa Y, Koga K, Tamegai T, Kitazawa K (1988) Proton NMR in degraded powder of $YBa_2Cu_3O_{7-\delta}$. Jpn J Appl Phys **27**: 1652-1657.

Rothman SJ, Routbort JL, Welp U, Baker JE (1991) Anisotropy of oxygen tracer diffusion in single-crystal $YBa_2Cu_3O_{7-\delta}$. Phys Rev B **44**: 2326-2330.

Salvador P, Fernandez-Sanchez E, Garsia Domingues JA, Amador J, Cascales C, Rasines I (1989) Spontaneous O release from $YBa_2Cu_3O_{7-x}$ high-T_c superconductor in contact with water. Solid State Commun **70**: 71-73.

Shiraishi K (1989) Irradiation effect in $Ba_2YCu_3O_{7-x}$ superconductor. J Nucl Mater **169**: 305-313.

Takenaka K, Mizuhashi K, Takagi H, Uchida S (1994) Interplane charge transport in $YBa_2Cu_3O_{7-y}$: Spin-gap effect on in-plane and out-of-plane resistivity. Phys Rev B **50**: 6534-6537.

Tikhonov AN, Arsenin VYa (1986) Methods of incorrect problem solution. Nauka, Moscow (in Russian).

Tsukui S, Yamamoto T, Adachi M, Shono Y, Kawabata K, Fukuoka N, Nakanishi S, Yanase A, Yoshioka Y (1991) Direct observation of O tracer diffusion in a $YBa_2Cu_3O_y$ single crystal by secondary ion mass spectrometry. Jpn J Appl Phys **30**: L973-L976.

Umansky VE, Solov'ev SA, Konnikov SG, Karmanenko SF, Kosogov OG (1990) Imaging of high-T_c superconducting film spatial inhomogeneities by low temperature scanning electron microscopy. Mater Lett **9**: 417-420.

Zhao R, Myhra S (1994) Environmental degradation of $YBa_2Cu_3O_{7-x}$. A descriptive and predictive model. Physica C **230**: 75-81.

Discussion with Reviewers

O.H. Aucieollo: How did you determine that there was no oxygen release when investigating the rate of relaxation? Did you do any mass spectrometry or optical spectroscopy?

Authors: We did not used any direct measurements to study oxygen release. Therefore, the possibility of oxygen release cannot be completely excluded. In particular, the fact that R(T) dependence of YBaCuO film exposed to water did not restore to its original form (see Fig. 15b) may be attributed to the oxygen release. However, the results on the anisotropy of oxygen diffusion and the relaxation of R(T) curves in vacuum suggest that it is not the key mechanism responsible for the film degradation.

O.H. Aucieollo: Is Figure 14 showing an evidence of a percolation mechanism for the transition from the non-superconducting to the superconducting state across the whole film?
Authors: The evidence of a percolation mechanism is provided by the results presented in Figures 7d, 7e and 7f. However, it should be taken into account that the data were obtained by a technique with a spatial resolution of about 1-2 μm. On a nm-scale, the percolation pattern may be different.

M.G. Norton: The authors imply that the composition of the film can be determined by backscattered electron imaging (BSEI). This may not be so. I am not sure that by BSEI, one could identify regions of the $YBa_2Cu_4O_x$ phase from regions of the $YBa_2Cu_3O_x$ phase, for example. And certainly, one could not identify regions of small changes in oxygen stoichiometry.
Authors: We do not mean that composition can be precisely determined in BSE mode, but that some additional information can be obtained by the study in this mode, in particular, the inclusions with substantially different composition can be separated ($BaCuO_2$, CuO). We agree that the difference in oxygen deficiency discussed in the paper could not be identified by this technique.

M.G. Norton: It is not clear to me that in the section **Water modification** that any new results have been obtained. It just seems that the authors are agreeing or disagreeing with existing theories and observations.
Authors: The new results can be summarized as follows: the process of water degradation of YBaCuO films is investigated with spatial resolution of 1-2 μm; the evolution of T_c-ensemble corresponding to more than 1000 fragments for each sample during storage in water is observed; and the data obtained indicate that water modification of the film results from hydrogen penetration into the film rather than oxygen out-diffusion.

M. Rautureau: What is the detection level of noise?
Authors: Since the sample is the part of the detecting system, the noise level depends on many parameters, such as: temperature, sample quality, width and length of the microbridge, and resistivity of the film. In our measurements, the noise never exceeded 10% of the signal level.

M. Rautureau: What is the structure of $YBa_2Cu_3O_7$?
Authors: The graphic structure of $YBa_2Cu_3O_7$ has been presented by, for example, Hazen *et al.* [Hazen RM, Finger LW, Angel RJ (1987) Crystallographic description of phases in the Y-Ba-Cu-O superconductor. Phys Rev **B35**: 7238-7241].